Journal of Cleaner Production 417 (2023) 138005

Contents lists available at ScienceDirect

Journal of Cleaner Production

journal homepage: www.elsevier.com/locate/jclepro

Phase change materials incorporation into 3D printed geopolymer cement: A sustainable approach to enhance the comfort and energy efficiency of buildings

Sahand Rahemipoor [a], Masoud Hasany [a], Mohammad Mehrali [b], Kristoffer Almdal [c], Navid Ranjbar [a], Mehdi Mehrali [a,*]

[a] Department of Civil and Mechanical Engineering, Technical University of Denmark, 2800, Kgs Lyngby, Denmark
[b] Faculty of Engineering Technology, Department of Thermal and Fluid Engineering (TFE), University of Twente, 7500, AE Enschede, the Netherlands
[c] Department of Chemistry, Technical University of Denmark, 2800, Kgs Lyngby, Denmark

ARTICLE INFO

Handling Editor: Liu Yu

Keywords:
Geopolymer
Microencapsulated PCM
3D printing
Fly ash
Phase change materials

ABSTRACT

The advent of 3D printing has revolutionized conventional construction, offering cost-effective and fast construction of complex structures. Nevertheless, there remain challenges to be addressed regarding the effective integration of functional additives into 3D printing construction materials. Herein, we present a straightforward and environmentally friendly approach to promote sustainable buildings while reducing energy consumption. This is achieved by integrating Macroencapsulated Phase Change Materials (MEPCM) into a 3D printable geopolymer paste (GPP) derived from fly ashes. The research followed a systematic methodology, encompassing the assessment of fresh and hardened properties of geopolymer pastes with varying amounts of MEPCM, analyzing their thermal properties, and investigating the thermal performance by printing miniature houses without and with 20 vol% MEPCM. Notably, MEPCM demonstrated its dual functionality as a thermal energy management component and a viscosity modifier for 3D printable geopolymer paste. Overall, this study paves an innovative path toward sustainable construction, highlighting the significance of energy efficiency and waste reduction.

1. Introduction

The increasing world population, economic growth, and industrialization have resulted in higher global energy demand (Singh et al., 2021). Carbon-based fossil fuel plays a big role in the worldwide energy supply and is the primary cause of global climate change and air pollution (Anisur et al., 2013; Shchukina et al., 2018). The buildings currently account for about 40% of global energy consumption and ~40% of CO_2 emissions (Du et al., 2021; Iten and Liu, 2014). Given that ~60% of building energy consumption accounts for heating and cooling systems, alternative approaches to regulating the temperature of buildings without auxiliary energy input are a strategic target for sustainable global development, particularly in thermal energy management and carbon footprint (Kasaeian et al., 2017). In recent years, there has been significant progress in utilizing phase change materials (PCMs) for thermal energy storage (TES) in order to enhance energy performance in various applications. These applications include photovoltaic (PV) panels, solar energy systems for hot water generation, heat exchangers, parabolic dish systems, thermo-electric generators, building walls, and more. (Ahmed et al., 2022; Jurčević et al., 2022; Palmer et al., 2023; Senthil et al., 2022). In buildings, PCMs can reduce reliance on mechanically assisted heating and cooling systems like heating, ventilation, and air conditioning (HVAC). By leveraging the thermal energy storage capabilities of PCMs, buildings can effectively regulate temperature and reduce the need for excessive use of HVAC, resulting in saving energy and improving overall efficiency (Chang et al., 2023; Milián et al., 2017). To put it simply, PCMs can reversibly store and release significant thermal energy in the form of latent heat during the melting and solidification phase transition in small temperature intervals (Akhiani et al., 2022; Han et al., 2022; Mehrali et al., 2013; Yan et al., 2022; Zhang et al., 2022, 2023). Different techniques are recommended to integrate PCMs into the construction building materials, including direct incorporation, shape-stabilizing, or microencapsulation (Wahid et al., 2017). Although direct incorporation and shape-stabilizing PCMs have lower operating costs, they suffer from drawbacks such as leakage into the environment and losing their ability

* Corresponding author.
E-mail address: meme@dtu.dk (M. Mehrali).

https://doi.org/10.1016/j.jclepro.2023.138005
Received 7 March 2023; Received in revised form 21 June 2023; Accepted 5 July 2023
Available online 6 July 2023

after a few cycles (Rao et al., 2018). A common approach to address these issues is to use microencapsulated phase change materials (MEPCM) (Dehmous et al., 2021; Erdem and Gürbüz, 2019; Latibari et al., 2015). The MEPCM method has the privilege of engulfing small solid or liquid particles with a solid shell, which prevents the leakage of PCMs from their location, reduces the interference toward phase-change behaviors from building materials, and increases the heat-transfer area (Al-Absi et al., 2022; Tyagi et al., 2016; Tyagi and Buddhi, 2007). These properties make MEPCM ideal for use as a TES system in building sectors (Cabeza et al., 2007; Lucas et al., 2013).

Conventional techniques for constructing building structures also need to be reshaped to achieve more energy reduction and provide flexibility to create complex geometries, such as the non-load bearing structures of buildings, allowing for PCMs to incorporate into indoor building structures (Lowke et al., 2018). To achieve this grand goal, auspiciously, the convergence of revolutionary three-dimensional (3D) printing technologies and construction materials change over the past decade has gradually brought a new sustainable scenario to replace the traditional building and construction processes (Ma et al., 2021). Among different 3D printing methods, extrusion-based 3D printing is the most affordable and widely adopted in the construction industry due to its low cost, user-friendly, and capability to tailor cement ink composition (Li et al., 2020). To achieve the best possible cement ink composition for use in extrusion-based 3D printing, flowability, extrudability, buildability, and open time, along with hardened properties, are crucial points that must be taken into consideration (Paul et al., 2018). Although Portland cement-based inks are one of the most remarkable and versatile in the 3D printing construction industry, they suffer from a negative environmental impact due to the process CO_2 emissions associated with production (Zhuang et al., 2016). One way to remedy this issue is to use and develop geopolymer-based cement, which also has additional features like slight drying shrinkage, high fire resistance, and superior acid resistance (Rifaai et al., 2019). In simple terms, geopolymer-based cement is produced through the alkaline activation of amorphous aluminosilicate materials in fly ash or bio ash (Pilehvar et al., 2019a; Singh et al., 2019). Since fly ash or bio ash are cheap and readily available industrial waste materials, for this reason, such waste materials-based geopolymers can considerably reduce CO_2 emissions in the construction industry and can be more affordable than Portland cement (Brooks et al., 2022; Cui et al., 2022a; Hao et al., 2022; Liu et al., 2022; Shahzad et al., 2021).

In this study, we have taken a novel approach to tackle the aforementioned limitations and offer sustainable/green buildings that consume less energy. Our method involves incorporating MEPCM into a 3D printable geopolymer matrix, which is derived from fly ashes. We have developed a straightforward, environmentally friendly, and cost-effective procedure to achieve this integration.

In pursuit of our objective, we diligently followed a step-by-step approach, which encompassed the following procedures:

i. Assessing the fresh properties of the geopolymers paste with different amounts of MEPCM, thoroughly examining its characteristics in its initial state.
ii. Evaluating the hardened properties of the 3D-printed geopolymers, including an analysis of their morphology, mechanical properties, and comprehensive material characterization.
iii. Conducting thermal analysis on geopolymer pastes with varying quantities of MEPCM.
iv. Investigating the thermal performance of geopolymer pastes by printing two miniature houses based on geopolymer without and with the highest proportion of MEPCM in terms of indoor and surface temperatures in simulated conditions.

By meticulously executing each of these steps, we were able to comprehensively analyze the geopolymer matrix and its incorporation of MEPCM, thereby advancing our understanding of the material's properties and thermal behavior. Furthermore, our findings reveal that MEPCM serves a significant function as a viscosity modifier for 3D printable geopolymer paste (GPP), in addition to its thermal energy management properties. Notably, this study shows that the harsh condition of geopolymerization due to its high pH does not affect the performance and structure of MEPCM. In summary, this study contributes to the advancement of 3D printing construction by introducing a new dimension, while simultaneously paving the way for sustainable buildings. By reducing energy consumption and the use of waste materials, our work offers promising opportunities in the field of sustainable construction.

2. Materials and methods

2.1. Materials

2.1.1. Fly ash

Class F fly ash (FA) from HOFOR Amagerværket was utilized to prepare geopolymer paste. FA chemical composition was determined by S8 Tiger 3 KW X-ray Fluorescence (XRF) which is demonstrated in Fig. 1a. FA particle size distribution was determined using a Malvern 3000 laser diffraction particle size analyzer as shown in Fig. 1b.

2.1.2. Activation solution

The activation solution was obtained by mixing sodium hydroxide pellet (purchased from INOVYN) and water to get an 8M solution before adding to the sodium silicate solution (consisting of 7.8–8.2 wt% SiO_2 and 26.6–27.0 wt% Na_2O) which was purchased from S.Sørensen-Thisted. The weight ratio of sodium silicate solution to sodium hydroxide solution for all mixtures was 15:2 (Ranjbar et al., 2021).

2.1.3. Encapsulated PCM

In this study, a slurry commercial microencapsulated PCM (MikroCapsPCM25-slurry) was utilized. This MEPCM consists of paraffin wax as the core and Melamine-formaldehyde as the shell and its TGA (TA TGA Q500 Thermogravimetric analyzer (USA)) and DTG analysis is shown in Fig. 1e. Based on the data provided by the supplier, MEPCM also has a particle size in the range of 1–20 μm, as its SEM image conveys (Fig. 1f). MEPCM melting point and latent heats were ~19.8 °C and ~139.2 J/g, respectively, which were obtained using a TA DSC Q200 Differential Scanning Calorimeter (DSC, USA) (Table 2).

2.2. Mixing and printing procedures

As presented in Fig. 2, in the first step, a certain amount of MEPCM slurry with additional water and fly ash was mixed and dried at room temperature to obtain GPP with 30 vol% MEPCM (FA-30%MEPCM) powder. Then, five different compositions of mixtures (0, 5, 10, 15, and 20% volumetric MEPCM) were prepared by adjusting and mixing (10 min) a certain amount of FA and FA-30%MEPCM. Finally, an alkaline activator was added to those powders and after 5 min of mixing, different geopolymer pastes (GPP) were obtained. The ratio of the activator solution to raw FA for all mixtures was 0.6 (Table 1).

To print GPPs, an HYREL 3D printer with an SR motor, equipped with a piston cartridge with a capacity of 60 ml and various nozzles, was utilized by operating with Repetrel software. For Printing different patterns, GPP-20% was considered to show the printability of this mixed design with 1.5, 1.6-, and 4.5 mm nozzles. To produce samples proper for mechanical tests and other analyses, a rectangular nozzle (20 × 4 mm) was used to extrude the multilayer beams.

Firstly, each mixture, after 5 min of mixing, was transported into a syringe. Each specimen with six layers had a 90 mm length and 20 mm height and was constantly printed with the 300 mm/min travel speed. In this study, all mixed designs were printed 20 min after the first printable time. Fig. 2 briefly demonstrates the mixing and printing procedures of specimens.

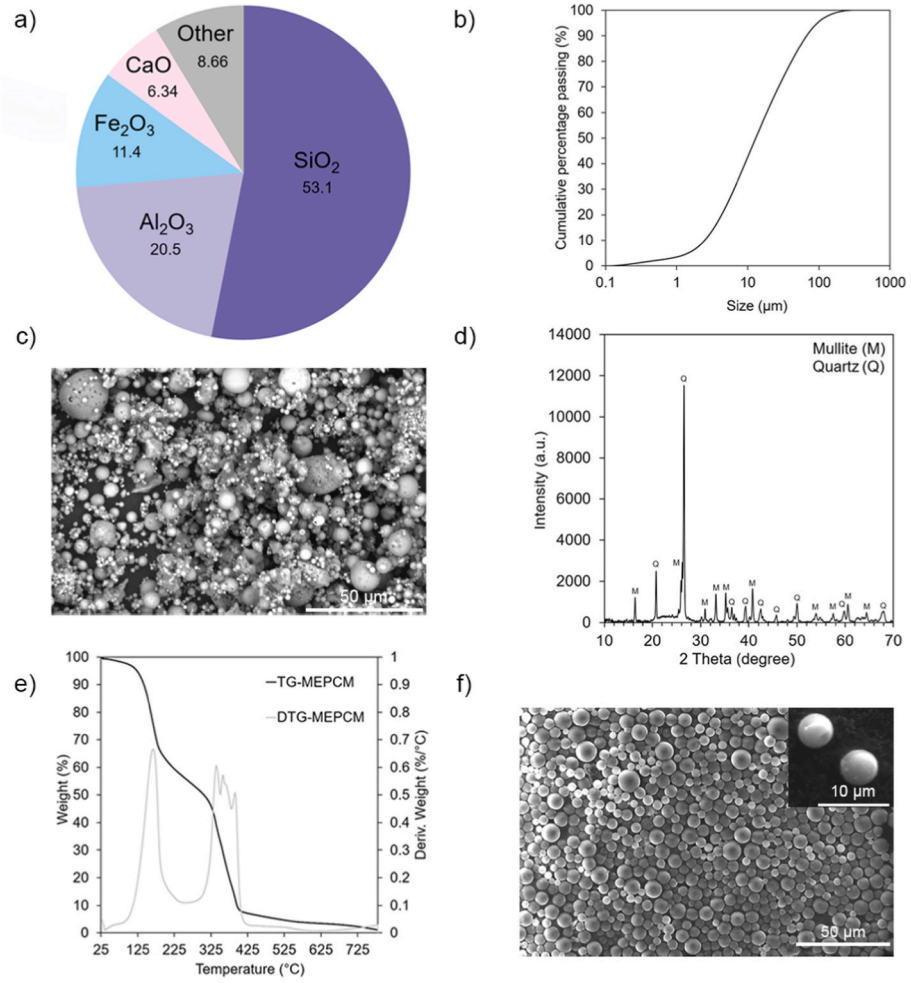

Fig. 1. a) Chemical composition of the FA in this study, b) Particle size distribution of the raw FA, c) SEM image of FA, d) X-ray diffraction pattern of the raw fly ash, e) TGA and DTG analyses of MEPCM, and f) SEM image of MEPCM.

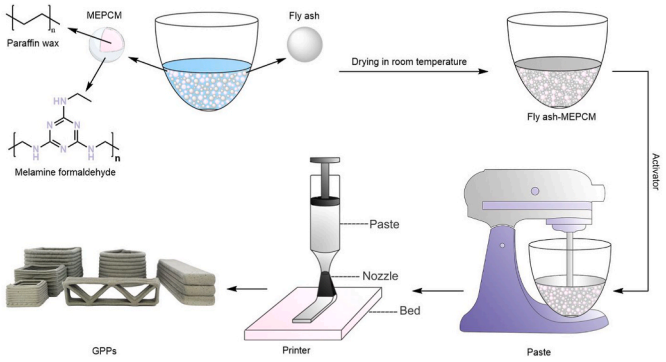

Fig. 2. Mixing and printing procedures of various GPPs.

2.3. Material characterization methods

2.3.1. Fourier transform infrared (FT-IR) spectroscopy

FT-IR spectroscopy test was conducted to observe the chemical compatibility of MEPCM with GPP. Accordingly, attenuated total reflectance-Fourier transform infrared (ATR-FTIR) on a PerkinElmer Spectrum 100 FTIR spectrometer was performed in the frequency range of 4000–600 cm^{-1} at a resolution of 4 cm^{-1} and 16 scans per sample.

2.3.2. Thermal conductivity

The printed GPP beams' thermal conductivity was tested using the hot wire method with a KD2 Pro thermal properties analyzer (Decagon Devices, SH-1 probe, USA) at room temperature (25 °C).

2.3.3. X-ray diffraction analysis (XRD)

Qualitative phase analysis of materials was measured using X-ray

Table 1
Mixture design of different GPPs with the ratio of 0.6 for activation solution to raw FA.

Composition	Name	FA-30%MEPCM (g)	Fly ash (g)	Activation solution (g)
0% volume MEPCM	GPP-0%	0	75	45
5% volume MEPCM	GPP-5%	12.5	62.5	43.9
10% volume MEPCM	GPP-10%	25	50	42.7
15% volume MEPCM	GPP-15%	37.5	37.5	41.6
20% volume MEPCM	GPP-20%	50	25	40.5

diffraction (XRD) Bruker AXS D8 Advance diffractometer. XRD patterns were operated at 40 kV and 40 mA from 10° to 70° with Cu Ka radiation at 25 °C. The step size and scanning rate were 0.0200 deg and 2s per step, respectively. Diffrac.Eva database was used to interpret phases, and the collection codes for mullite and quartz were 85–1460 and 40–1045.

2.3.4. Differential scanning calorimetry (DSC)

DSC by TA Instruments DSC Q200 was employed to assess each mixed design's thermal properties and thermal stability. Each sample was equilibrated in an aluminum pan at 20 °C, and all experiments were performed from 0 to 40 °C at a rate of 5 °C/min under continuous 50 ml/min N_2 gas purge. For the cyclic test, the temperature range was conducted from −5 to 35 °C in the same condition for 100 cycles.

2.3.5. Thermogravimetric analysis (TGA)

TGA by TA TGA Q500 Thermogravimetric Analyzer was employed to assess the thermal stability and effect of MEPCM on various GPPs at 28 days. All samples were heated from 30 °C to 800 °C under continuous 50 ml/min N_2 gas purge and at a ramping rate of 10 °C/min.

2.3.6. Microscopy

MEPCM were imaged in activator solution and water with a Zeiss LSM 700 confocal laser scanning microscope using green color. The micromorphology characteristics of GPP-0% and GPP-20% were studied using a scanning electron microscope (Quanta FEG 250 Analytical ESEM), which was operated with an accelerating voltage of 15 kV and a high vacuum chamber with the pressure of 10^{-2} Pa.

2.3.7. Setting time

The Vicat setting times of GPPs were determined based on ASTM C191 by a manual Vicat needle setup.

2.3.8. Rheological characterization

Rheological assessments of all mixed designs were performed after 10 min of mixing and exact printing time to obtain a comparison in the same condition and at printing time. To measure the rheological characters of all GPPs, Anton Paar Physica MCR 502 rheometer was used with a 25 mm parallel plate system (PP25). The distance between the plates was considered 2 mm, so it was at least eight times larger than the maximum particle size of the FA (0.211 mm). To maintain the same condition for GPPs, the temperature was stable at 23 °C utilizing temperature control systems P-PTD200 and H-PTD200. Data were recorded with Rheoplus/32 software version 2.65 (Anton PaarGmbH).

Three-step measurements were conducted. First, the samples were subjected to a high oscillatory pre-shearing of %5 strain with a frequency of 1 Hz for the 30s to bring all the samples into a similar measuring condition. Then the shear rate ramped from 0.2 to 30 s^{-1} in a logarithmic trend to measure 20 data points. The shear rate ramped down from 30 to 0.2 s^{-1} including 20 measurement points with a similar logarithmic distribution as in the last step. The descending curve was used in this study to analyze the rheological properties of the pastes after fitting with the linear Bingham (BH) model by Eq (1):

$$\tau = \tau_0 + \eta\gamma \quad (1)$$

In this formula, τ is the shear stress (Pa), τ_0 is the yield stress (Pa), η is the plastic viscosity (Pa·s), and γ is the shear rate (s^{-1}). The correlation coefficient (R^2) of all plots were above 0.975 which demonstrates that the matching degree between the experiment and fitted results in the Bingham model was reasonable.

2.4. Mechanical characterization methods

Compression and 3-point bending tests were performed for direct extrude-based printed and casted pastes of all mixed designs at room temperature and curing times of 7, 14, and 28 days. To determine the flexural strength of GPPs, Instron 8872 was employed with a 10 kN load cell and loadings rate of 0.1 mm/min. The dimension of printed GPPs was 20 × 21.6 × 90 mm^3 for the 3-point bending test. The 3D printed samples were cut into (20 × 20 × 20 mm^3) to measure the compression test by MTS 312.31A with 250 kN load cell and 0.5 mm/min loadings rate. At least six samples for compressive strength and four for flexural strength were measured, and the average values were reported.

2.5. Thermal performance testing

To investigate the MEPCM effect on the thermal performance of GPP, a humidity chamber (Memmert ICH110C) was deployed with a 48-h temperature program with a cyclic temperature change in the range of 15–30 °C for every 12 h and 50% constant humidity. In this test, two cubic miniature houses with dimensions of 40 × 40 × 40 mm^3 and thickness of 5 mm were printed with GPP-0 and GPP-20 vol% MEPCM as reference houses and PCM houses, respectively. For each miniature house, a sensor of temperature recording set up was placed inside the house, and a printed roof was stocked with fresh paste. The temperature recording device recorded the temperature of those houses every second. An infrared camera (OPTRIS PI 640 IR-camera) was utilized to monitor the surface temperature of printed miniature houses in another cycle in the humidity chamber.

3. Results and discussion

3.1. Characterization of fresh different GPPs

In line with our previous work, the GPPs are classified into three categories based on their printability: too flowable (Fig. 3a 1), printable (Fig. 3a 2 to 4), and not extrudable (Fig. 3a 5) (Ranjbar et al., 2021). Moreover, the printability window as a function of time for all GPPS is shown in Fig. 3b. As observed in Fig. 3b, the printing time was reduced as the amount of MEPCM in the mixture increased (from GPP-0% to GPP-20%) (Alghamdi and Neithalath, 2019). A further point to note is that GPP-15% and GPP-20% didn't have a flowable mode; after mixing the paste, they were printable (Romagnoli et al., 2014). To put it another way, the more MEPCM mixture there was, the less period mixture could be printed.

Fig. 3b 2,3 and 4 indicate that printing quality decreased gradually due to increased rheological properties of the fresh matrices, e.g., yield stress and viscosity (Panda et al., 2019). These results indicate that over time yield stress and plastic viscosity of all mixtures are increased, and through enough time, specimens that are not initially printable can become printable, see Fig. 3c, d, and e (Ranjbar et al., 2023; Roussel, 2018).

Fig. 3f illustrates the change in GPPs Vicat setting times as a function of different amounts of MEPCM. As the amount of MEPCM in the solid phase was increased, the initial and final setting times were sped up. We speculate that this result is due to water absorption on the surface of MEPCM and the surfactant that the supplier used for stabilizing MEPCM in the slurry, which reduced the liquid phase in the paste and thereby increased viscosity. Due to this, it reduced the speed of geopolymerization after the initial stage; as the first decrease in penetration depth for all specimens was between 380 and 410 min after mixing, but by increasing the amount of MEPCM, initial and final setting times were raised up to 18% and 47%, respectively. This phenomenon may impact the mechanical properties of GPPs due to the reduction in the speed of the geopolymerization process in the hardening stage (Pilehvar et al., 2019b, 2020a).

3.2. Microstructures of printed geopolymer with 20% and without MEPCM

In view of the fact that the activator for geopolymers consists mainly

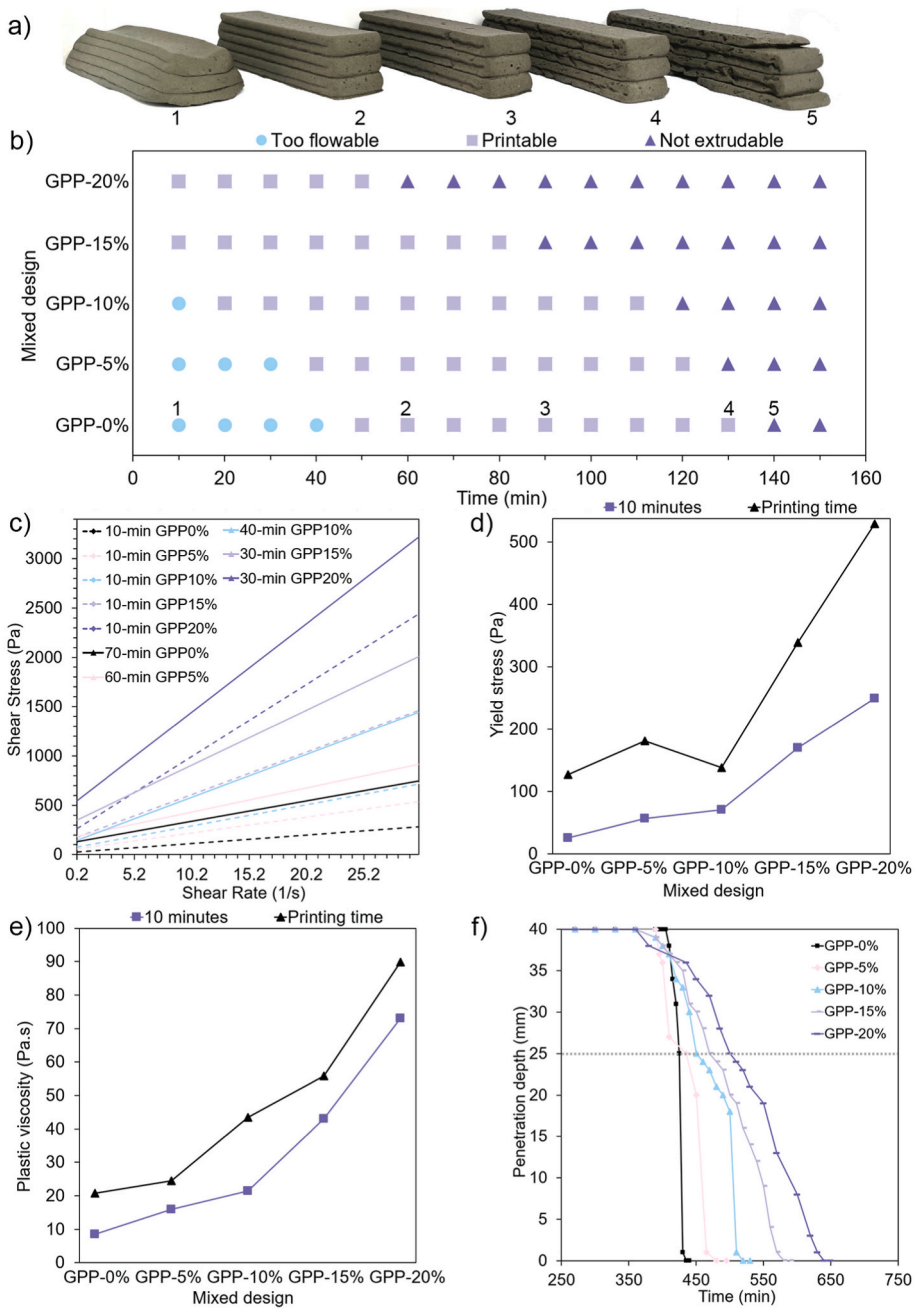

Fig. 3. Properties of fresh, different geopolymer pastes (GPPs) with various amounts of MEPCM; a) visual inspection of different printed modes according to printability window b) printability window as a function of time, c) shear stress versus shear rate fitted by Bingham, d) yield stress plot, e) plastic viscosity plot, and f) Vicat setting time.

of sodium hydroxide with a high pH, the first concern of using micro-encapsulated PCM is the destruction of the shell and the loss of the core-shell structure, like MEPCM with silica shell. Moreover, leaking paraffin into the concrete matrix following several cycles of melting and freezing would also be undesirable. Since the MEPCM shell used in this study is composed of an amino resin-based polymer (melamine-formaldehyde), these phenomena were not observed due to the resistance of the amine group to alkaline solutions.

In order to confirm this hypothesis, two solutions of MEPCM in water (Fig. 4a) and an activator (Fig. 4b) at a concentration of 1 mg/ml were prepared and left for a day at room temperature. The structure of MEPCM in the solutions was then imaged and analyzed using a fluorescence microscope. Based on a comparison of Fig. 4a and b, it can be seen that the concentrated alkali solution did not destroy the morphology of the MEPCM.

The cross-sectional SEM images of GPP-0% (Fig. 4c and d) and GPP-20% (Fig. 4e and f) show after 28 days of printing. As can be seen, there is no obvious distinction between GPP-0% and GPP-20% in the geopolymer matrix. This fact can be interpreted to be due to the low chemical reactivity of melamine-formaldehyde in the shell, which did not react with the geopolymer binder under this condition, even though MEPCM in GPP-20% may influence the mechanical and thermal properties. Fig. 4e and f also reveal that the MEPCM retained its spherical shape within the geopolymer matrix, suggesting that the MEPCM can maintain its structure during the geopolymerization process (Cao et al., 2018; Pilehvar et al., 2020b).

3.3. Material and mechanical properties of all printed GPPs

Three characterization methods were used to characterize MEPCM

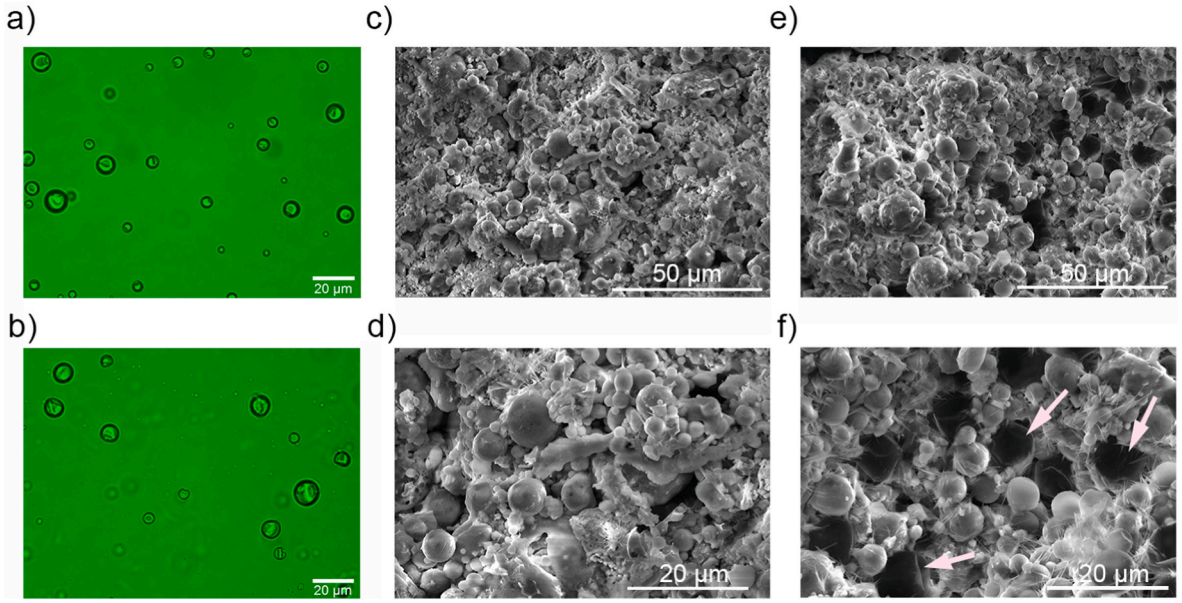

Fig. 4. Optical images of MEPCM in water and activator (a,b) and SEM images of the fractural surface of printed GPP-0% (c, d) and GPP-20% (e, f) after 28 days.

ineffectiveness in chemical reactions and geopolymerization processes. In the first step, FT-IR analyses were considered for this purpose. Fig. 5a demonstrates the FTIR spectra of MEPCM and all GPPs. In the MEPCM spectrum, absorbances between 3100 and 3600 cm^{-1} represent the stretching vibrations of primary amine. The absorptions at 2853, 2921, and 2958 cm^{-1} corresponded to the C–H stretching vibration in paraffin and melamine-formaldehyde. Peaks at 1545, 1492, and 1336 cm^{-1} were attributed to in-plane triazine ring vibration. The bending vibration of C–H was observed at 1465 cm^{-1}. Furthermore, C–O stretching vibrations were detected at 1156 and 1006 cm^{-1}, respectively. The peak at 811 cm^{-1} is related to out-of-plane triazine ring vibration (Jiang and Liu, 2015; Merline et al., 2013; Wang et al., 2012).

In GPP-0%, a broad peak at 998 is assigned to the asymmetric stretching vibration of Si–O–Si. Stretching and bending vibration of O–H groups were revealed at 3450 and 1640 cm^{-1} respectively (Ranjbar et al., 2015). In GPPs with the MEPCM, as expected, by increasing the percentage of MEPCM in the mixed design, the intensity of absorbance peaks corresponding to the MEPCM was increased compared to the absorbance intensity of peaks corresponding to geopolymer. FT-IR results indicate that MEPCM does not participate in geopolymerization or react with the materials in the mixture, as no new peak is identified.

In the next step, Thermogravimetric analysis (TGA) on GPPs (Fig. 5b) and MEPCM (Fig. 1e) was used to study the influence of MEPCM on geopolymer. Also, the derivative thermogravimetry (DTG) of MEPCM and all GPPs were shown in Figs. 5c and 1e for a clear designation of the temperature borders during various decomposition processes. As observed, the first mass loss in the range of 35 °C–100 °C in TGA and peaks in the range of 55 °C–75 °C in DTG, are corresponded to free water in all samples. The procedure of paraffin mass loss began at ~90 °C and ended at ~250 °C. The second peak in DTG between 120 °C and 140 °C is therefore attributable to the decomposition of paraffin wax in the MEPCM. Consequently, since the decomposition of melamine-formaldehyde occurs at temperatures between 270 °C and 420 °C, the last peaks in the DTG, about 350 °C, correspond to the decomposition of the shell, as can be seen in Fig. 5c (Djamai et al., 2019; Hao et al., 2022; Jiang and Liu, 2015; Parameshwaran et al., 2021).

Based on the TGA results, it can be concluded that there is no interaction between the MEPCM and matrix, as no new peaks exist in the pure MEPCM or GPP-0% runs. Finally, qualitative phase analysis of raw fly ash and printed GPP-0 and 20% were demonstrated in Fig. 1d and 5d, respectively. The results also prove that MEPCM does not affect geopolymerization reaction, since no difference in XRD patterns was observed between GPP-0% and GPP-20%, as shown in Fig. 5d.

To study the impact of MEPCM on the mechanical properties of GPPs, the compressive strength and flexural strengths were measured 7, 14, and 28 days after mixing (Fig. 5e and f). Increasing the percentage of MEPCM in the paste leads to having lower compressive and flexural strengths. Two factors may explain this trend; first, MECPM has low mechanical strength and hardness, which makes it easy to break with little force; second, as discussed above, MECPM does not participate in geopolymerization and weakly bonds with matrix particles. Moreover, microporosity and the gap between the MEPCM and matrix particles could also be contributing factors to the reduction in mechanical properties (Cui et al., 2022b; Pilehvar et al., 2020b).

According to Fig. 5e, comparing the compressive strength of 7 days and 28 days specimens indicates that MEPCM had a lower effect on early-age geopolymerization by up to 62% and 44% reduction in compressive strength, respectively. The seven-day trend in Fig. 5f illustrates that MEPCM does not significantly affect flexural strengths; in other words, values are in the same range. Furthermore, the reduction in 28 days of flexural strengths was up to 36%, which reveals that MEPCM affects flexural strengths less than compressive strength (Pilehvar et al., 2017; Shadnia et al., 2015; Shahzad et al., 2021).

It is concluded that, although the compressive strengths of all GPPs do not meet load-bearing concrete requirements, however, according to ASTM C129-17, non-loadbearing masonry units should achieve 4.14 MPa compressive strengths, and all samples have compressive strengths above that (Hassan et al., 2019a, 2019b). Furthermore, both charts of mechanical properties demonstrate that a higher percentage of MEPCM caused to decline in the hardening evolution of geopolymer during the time, in which 14 days results are getting closer to 7 days instead of 28 days from GPP-0% to GPP-20%. This is probably because occupied spaces of MEPCM in the mixture do not allow geopolymer clusters to continue polymerization as fast as the absence of MECPM in geopolymer, and thus the presence of MEPCM reduces the process's speeds.

3.4. Thermal properties of all materials

The thermal conductivity of MEPCM and all GPPs at room temperature are summarized in Fig. 6a. As it conveys, there is no significant change in various GPPs with the range of 0.50 up to 0.54 W/(m.K), although the thermal conductivity of MEPCM was much lower than geopolymers by 0.14 W/(m.K). Thus, the thermal conductivity does not significantly change when MEPCM is incorporated into a geopolymer

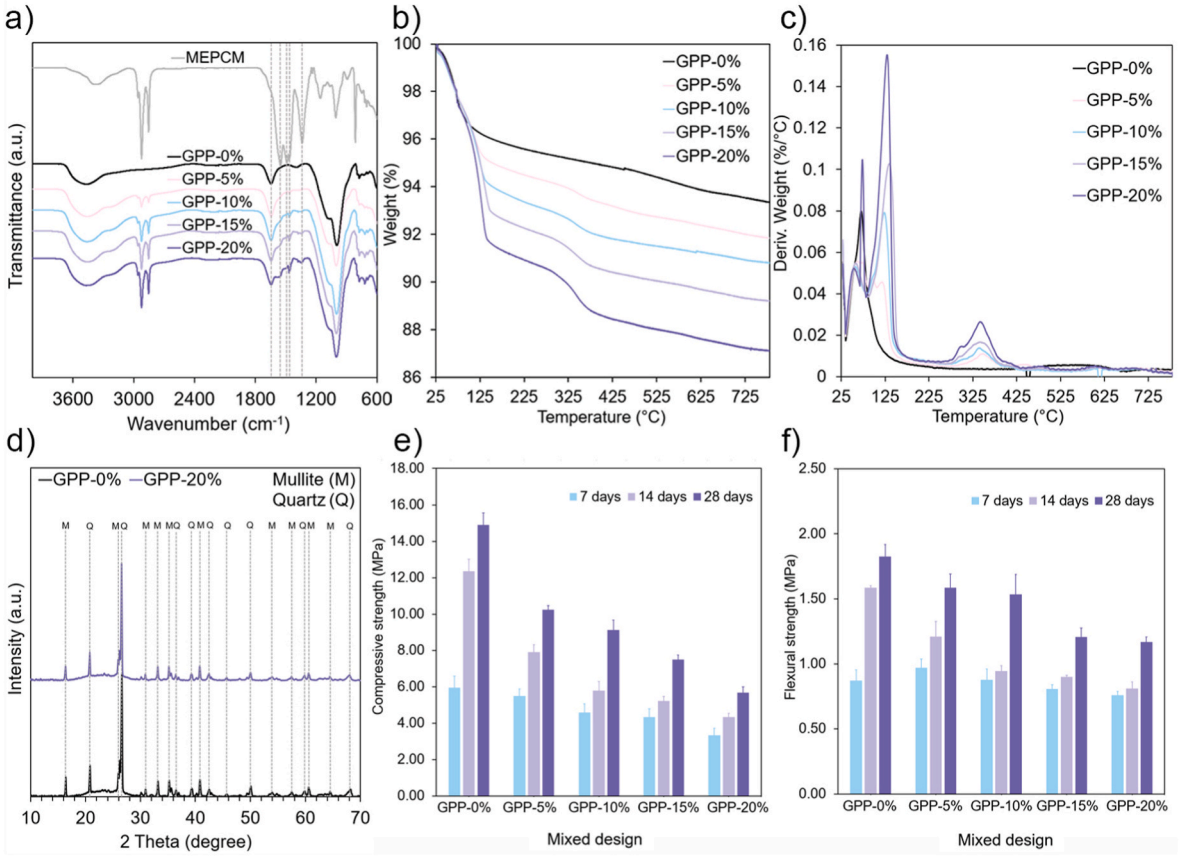

Fig. 5. FT-IR of all materials (a), TGA (b), and DTG (c) of GPPs after 28 days of printing, XRD patterns of GPP-0% and GPP-20%, and compressive strengths (e) and flexural strengths (f) of all printed GPPs after 7,14, and 28 days of printing time.

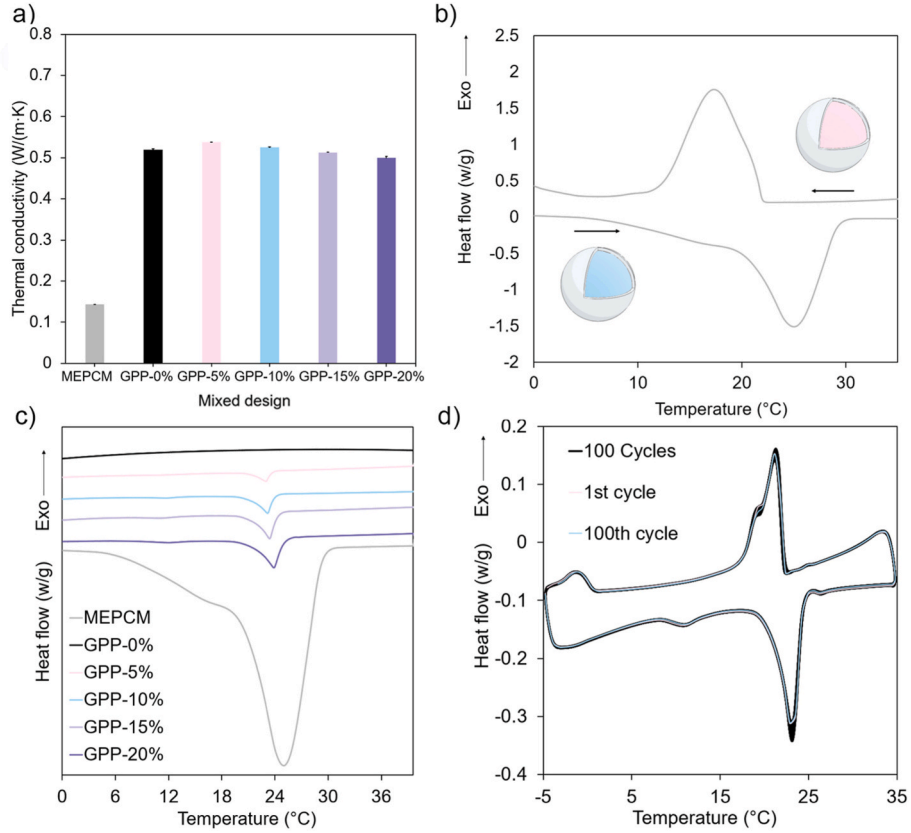

Fig. 6. Thermal conductivity (a), DSC curves of MEPCM (b) and GPPs (c), and DSC curves of 100 cycles of GPP-20% (d).

Table 2
Calculated latent heat and results of DSC analyses of MEPCM and all GPPs.

Mixed design	ΔH_{calc} (J/g)	ΔH_{exp} (J/g)[1]	T_m (°C)	T_{peak} (°C)
MEPCM	–	139.2 ± 2.1	19.79 ± 0.21	25.17 ± 0.38
GPP-0%	–	0	–	–
GPP-5%	2.20 ± 0.03	2.62 ± 0.03	20.95 ± 0.05	23.01 ± 0.04
GPP-10%	4.44 ± 0.07	4.84 ± 0.21	20.95 ± 0.01	23.18 ± 0.01
GPP-15%	6.72 ± 0.10	7.14 ± 0.22	21.23 ± 0.02	23.44 ± 0.04
GPP-20%	9.04 ± 0.14	10.01 ± 0.22	21.20 ± 0.06	23.87 ± 0.02

ΔH_{exp} represents the latent heat of samples obtained from the DSC curve.

system up to 20 vol%. Consequently, Integrating MEPCM into geopolymer up to 20 vol% does not significantly change the thermal conductivity (Brooks et al., 2022; Hao et al., 2022). Hence, if these materials are utilized as construction materials for walls, they will not contribute to an increase in heat exchange with the environment or an increase in energy loss. Indeed, when the thermal conductivity of building materials decreases, less energy is needed to maintain comfortable conditions inside the building.

Additionally, to investigate the thermal performance of GPPs, DSC analyses were used to measure the latent heat of each mixed design. The DSC curves and results of MEPCM and GPPs after 28 days of printing time were demonstrated in Fig. 6b and c and Table 2, respectively. As expected, latent heats of GPPs were increased by increasing the percentage of MEPCM in mixed designs (Wei et al., 2017). However, they did not wholly follow the calculated latent heats of mixed designs, which are obtained by Eq (2):

$$\Delta H_{calc} = \Delta H_{MEPCM} \times \frac{W_{MEPCM}}{(W_{MEPCM} + W_{Activator} + W_{Fly\ ash})} \quad (2)$$

Where ΔH_{calc}, ΔH_{MEPCM} and W represent the GPP latent heat, the MEPCM latent heat, and the weight of components in the mixture, respectively (Ramakrishnan et al., 2015). This unfitting may have two reasons: first, after 28 days, some water in the activator is evaporated and $W_{Activator}$ should be smaller than the initial value, second, specimens are not a perfectly homogeneous mixture, because of its nature(Parameshwaran et al., 2021).

Furthermore, the thermal cyclic test was conducted to ensure that MEPCM would remain unchanged over the course of day and night. Fig. 6d illustrates the DSC curve of GPP-20% from the first to the 100th cycle. Based on these curves, the MEPCM retains its structure in the geopolymer structure when temperatures are cycled, if the shells of MEPCM had been torn, the DSC results would be changed after 100 cycles (Gencel et al., 2022b).

Finally, the thermal properties of GPP-20% were compared to those of previous studies, as shown in Table 3.

Table 3
Thermal properties comparison of PCM integrated into geopolymer.

PCM in solids	ΔH_{exp} (J/g)[1]	T_m (°C)	Thermal conductivity (W/(m. K))	Reference
30 vol%	11.37	23.7	–	Ramakrishnan et al. (2021)
30 wt%	6.57	18.30	0.375	Gencel et al. (2022a)
20 vol%	6.40	19.8	0.84	Haily et al. (2023)
16 wt%	24.74	27.27	0.51	Fang et al. (2023)
20 vol%	10.01 ± 0.22	21.20 ± 0.06	0.499 ± 0.01	This study

3.5. Thermal performance of printed GPP-20%

To show the effect of MEPCM in GPPs as a function of thermal performance, in the first step, the surface temperature of two miniature printed houses was studied. Those Houses (printed by GPP-0% as a reference and GPP-20% as a PCM house) were analyzed in a humidity chamber with a rising temperature program from 15 to 30 °C in 30 min and 60 min of standing temperature at 30 °C (heating process).

Later, an IR camera was applied to monitor the surface temperature of houses; see Fig. 7a and Video S1. Fig. 7b demonstrated that the GPP-0% house surface changing temperature was lower than the environment temperature. This observation is mainly because of the heat capacity of geopolymer during this fast temperature increase. Interestingly, the GPP-20% house indicated much lower environmental temperature sensitivity; Even the temperature difference between this house and the GPP-0% house was extremely considerable (the maximum temperature difference was 3.2 °C), see Fig. 7c. This difference is mainly due to the absorbing latent heat of MEPCM during the melting point of around 21 °C.

This study also was done as a cooling process by decreasing temperatures from 30 to 15 °C in 30 min and then resting for 70 min at 15 °C, See Video S2. Fig. 7d indicates the moment of the maximum temperature difference of those houses during the cooling process. According to Fig. 7e and f, the maximum temperature difference in this cycle was about 3.6 °C. This difference in maximums in cooling and heating processes is subjected to the difference in the melting and solidification profile of MEPCM, mainly due to the supercooling phenomenon of paraffin wax, and also can be observable in DSC curves (Mohseni et al., 2020; Ren et al., 2020).

For simulating temperature changes during the day and illustrating the effect of MEPCM on temperature regulation of the miniature printed house, a temperature cycle from 15 to 30 °C was considered. Accordingly, at first in the humidity chamber, the temperature was increased from 15 to 30 °C in 12 h as a function of daytime and then was reduced from 30 to 15 °C as a function of the night; see Fig. 7g, h, and i. As witnessed, the GPP-0% house completely follows the temperature program, while the GPP-20% house does not follow the temperature program in the time range of 300–600 min during the heating and 1000–1300 min during the cooling processes.

As a result, the temperature difference between the two houses reaches 1.2 °C in both the melting and solidification ranges of MEPCM during the cycle, notwithstanding that the walls in both houses were just 0.5 cm (Athukorallage et al., 2018; Essid et al., 2022). Consequently, within the rising environment temperature, MEPCM can prevent a temperature rise in the house by absorbing energy during the melting process (between 21 °C and 26 °C) and can prevent a temperature drop during falling environment temperature by releasing energy through the solidification process (between 19 °C and 24 °C). Since the speed of changing temperature in this simulation is much slower than in previous cycles, the difference in melting and solidification profiles was not observed.

Supplementary video related to this article can be found at https://doi.org/10.1016/j.jclepro.2023.138005

4. Conclusion

The research findings presented in this study contribute to the scientific value and application for 3D printing of geopolymer matrices incorporated with MEPCM. The conclusions drawn from the study are as follows:

- Increasing the amount of MEPCM in the geopolymer paste enhanced its yield stress and viscosity, resulting in a shift in the printability window. Additionally, higher percentages of MEPCM led to longer final setting times, with a 20-vol% MEPCM addition increasing the final setting time by up to 50%.

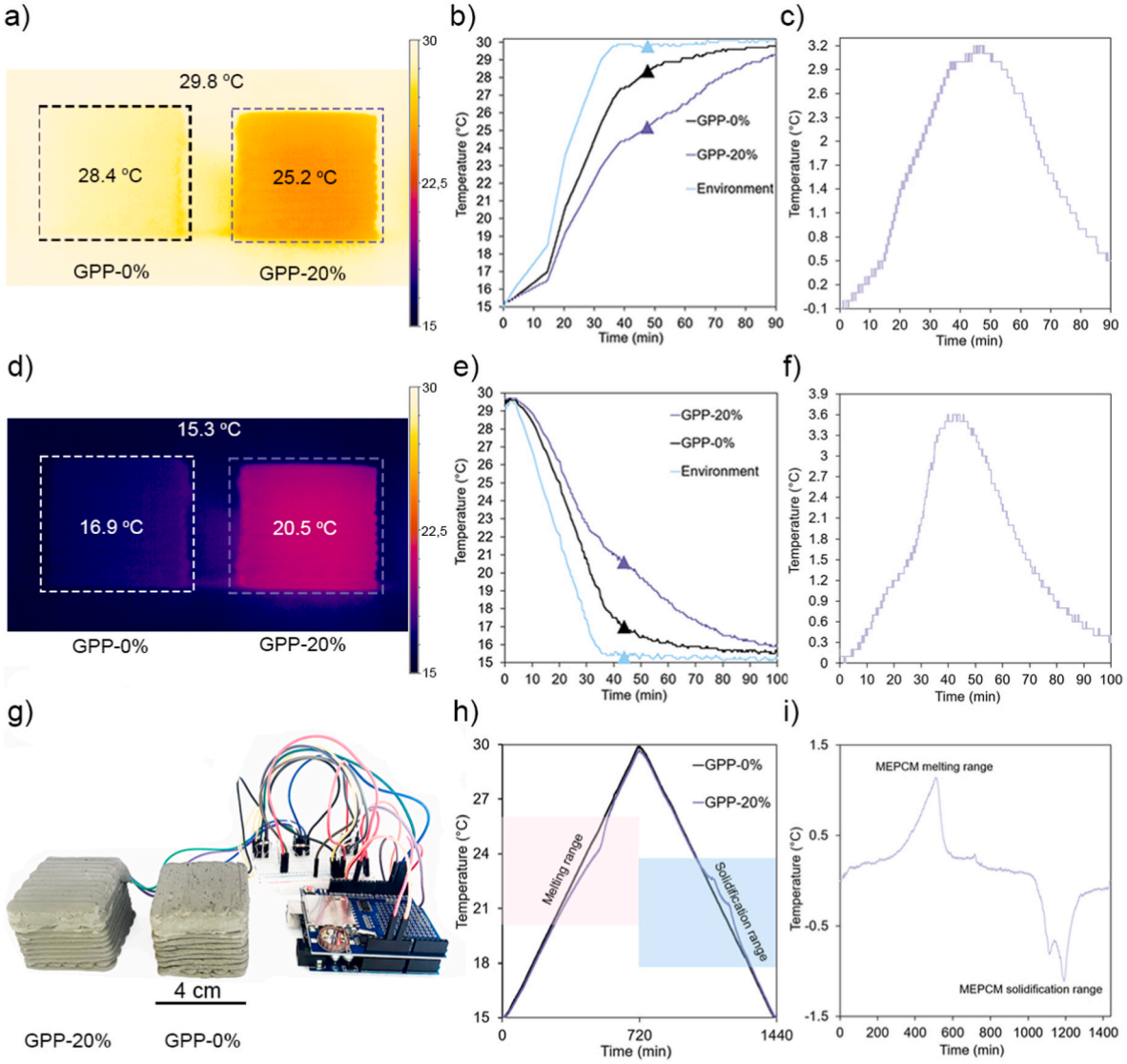

Fig. 7. IR images of the printed GPP-0% and GPP-20% houses in the maximum difference's moment (a, d), their temperature recorded (b, e), and temperature difference versus time between houses (c, f) during the heating and cooling processes, and those printed houses in which temperature sensors were inside (g), one-day cycle temperature profile of houses in the humidity chamber (h) and their temperature difference (i).

- MEPCMs demonstrated structural stability and resistance to the highly alkaline environment of geopolymerization. They did not participate in the chemical reaction of geopolymerization. However, the presence of MEPCM caused a decrease in the hardening evolution over time and resulted in a reduction of mechanical strength by approximately 60% in compressive strength tests after 28 days.
- The incorporation of MEPCM in the geopolymer matrix significantly improved thermal performance. The GPP with an additional 20 vol% MEPCM exhibited a latent heat of 10.01 ± 0.22 J/g. Notably, the thermal conductivity of the geopolymers was only slightly reduced by approximately 4%.
- Thermal cyclic testing revealed the stability of the MEPCM-incorporated geopolymer, as no significant changes were observed during temperature cycling, even after 100 cycles.

Future studies should focus on enhancing the mechanical performance of MEPCM-incorporated geopolymer. One potential avenue is exploring modifications to the MEPCM shell, such as incorporating silica to improve bonding with the geopolymer matrix. Additionally, optimizing the geopolymer composition may yield improvements in mechanical properties. Lastly, it is crucial to enhance the scaling up of MEPCM production in the construction sector. These areas warrant further investigation to expand the potential of MEPCM-incorporated geopolymer materials.

CRediT authorship contribution statement

Sahand Rahemipoor: Methodology, Validation, Formal analysis, Investigation, Visualization, Data curation, Writing - original draft, Writing - review & editing. **Masoud Hasany:** Investigation, Validation, Visualization, Writing - review & editing. **Mohammad Mehrali:** Investigation, Validation, Writing – review & editing. **Kristoffer Almdal:** Investigation, Writing – review & editing. **Navid Ranjbar:** Investigation, Validation, Writing – review & editing. **Mehdi Mehrali:** Conceptualization, Supervision, Investigation, Validation, Funding acquisition, Resources, Data curation, Project administration, Visualization, Writing - review & editing.

Declaration of competing interest

The authors declare that they have no known competing financial interests or personal relationships that could have appeared to influence

the work reported in this paper.

Data availability

Data will be made available on request.

Acknowledgment

This work was supported by research grants (00025460) from VILLUM FONDEN.

References

Ahmed, S.F., Rafa, N., Mehnaz, T., Ahmed, B., Islam, N., Mofijur, M., Hoang, A.T., Shafiullah, G.M., 2022. Integration of phase change materials in improving the performance of heating, cooling, and clean energy storage systems: an overview. J. Clean. Prod. 364 https://doi.org/10.1016/j.jclepro.2022.132639.

Akhiani, A.R., Cornelis Metselaar, H.S., Ang, B.C., Mehrali, Mehdi, Mehrali, Mohammad, 2022. Highly hydrophobic silanized melamine foam for facile and uniform assembly of graphene nanoplatelet towards efficient light-to-thermal energy storage. Mater. Today Energy 28. https://doi.org/10.1016/j.mtener.2022.101077.

Al-Absi, Z.A., Hafizal, M.I.M., Ismail, M., Awang, H., Al-Shwaiter, A., 2022. Properties of PCM-based composites developed for the exterior finishes of building walls. Case Stud. Constr. Mater. 16 https://doi.org/10.1016/j.cscm.2022.e00960.

Alghamdi, H., Neithalath, N., 2019. Synthesis and characterization of 3D-printable geopolymeric foams for thermally efficient building envelope materials. Cem. Concr. Compos. 104 https://doi.org/10.1016/j.cemconcomp.2019.103377.

Anisur, M.R., Mahfuz, M.H., Kibria, M.A., Saidur, R., Metselaar, I.H.S.C., Mahlia, T.M.I., 2013. Curbing global warming with phase change materials for energy storage. Renew. Sustain. Energy Rev. https://doi.org/10.1016/j.rser.2012.10.014.

Athukorallage, B., Dissanayaka, T., Senadheera, S., James, D., 2018. Performance analysis of incorporating phase change materials in asphalt concrete pavements. Construct. Build. Mater. 164, 419–432. https://doi.org/10.1016/j.conbuildmat.2017.12.226.

Brooks, A.L., He, Y., Farzadnia, N., Seyfimakrani, S., Zhou, H., 2022. Incorporating PCM-enabled thermal energy storage into 3D printable cementitious composites. Cem. Concr. Compos. 129 https://doi.org/10.1016/j.cemconcomp.2022.104492.

Cabeza, L.F., Castellón, C., Nogués, M., Medrano, M., Leppers, R., Zubillaga, O., 2007. Use of microencapsulated PCM in concrete walls for energy savings. Energy Build. 39, 113–119. https://doi.org/10.1016/j.enbuild.2006.03.030.

Cao, V.D., Pilehvar, S., Salas-Bringas, C., Szczotok, A.M., Valentini, L., Carmona, M., Rodriguez, J.F., Kjøniksen, A.L., 2018. Influence of microcapsule size and shell polarity on thermal and mechanical properties of thermoregulating geopolymer concrete for passive building applications. Energy Convers. Manag. 164, 198–209. https://doi.org/10.1016/j.enconman.2018.02.076.

Chang, Y., Yao, X., Chen, Y., huang, L., Zou, D., 2023. Review on ceramic-based composite phase change materials: preparation, characterization and application. Compos. B Eng. 254, 110584 https://doi.org/10.1016/j.compositesb.2023.110584.

Cui, H., Yu, S., Cao, X., Yang, H., 2022a. Evaluation of printability and thermal properties of 3D printed concrete mixed with phase change materials. Energies 15. https://doi.org/10.3390/en15061978.

Cui, H., Yu, S., Cao, X., Yang, H., 2022b. Evaluation of printability and thermal properties of 3D printed concrete mixed with phase change materials. Energies 15. https://doi.org/10.3390/en15061978.

Dehmous, M., Franquet, E., Lamrous, N., 2021. Mechanical and thermal characterizations of various thermal energy storage concretes including low-cost bio-sourced PCM. Energy Build. 241 https://doi.org/10.1016/j.enbuild.2021.110878.

Djamai, Z.I., Salvatore, F., Si Larbi, A., Cai, G., el Mankibi, M., 2019. Multiphysics analysis of effects of encapsulated phase change materials (PCMs) in cement mortars. Cement Concr. Res. 119, 51–63. https://doi.org/10.1016/j.cemconres.2019.02.002.

Du, K., Calautit, J., Eames, P., Wu, Y., 2021. A state-of-the-art review of the application of phase change materials (PCM) in Mobilized-Thermal Energy Storage (M-TES) for recovering low-temperature industrial waste heat (IWH) for distributed heat supply. Renew. Energy. https://doi.org/10.1016/j.renene.2020.12.057.

Erdem, S., Gürbüz, E., 2019. Influence of microencapsulated phase change materials on the flexural behavior and micromechanical impact damage of hybrid fibre reinforced engineered cementitious composites. Compos. B Eng. 166, 633–644. https://doi.org/10.1016/j.compositesb.2019.02.059.

Essid, N., Eddhahak, A., Neji, J., 2022. Experimental and numerical analysis of the energy efficiency of PCM concrete wallboards under different thermal scenarios. J. Build. Eng. 45 https://doi.org/10.1016/j.jobe.2021.103547.

Fang, Y., Ahmad, M.R., Lao, J.C., Qian, L.P., Dai, J.G., 2023. Development of artificial geopolymer aggregates with thermal energy storage capacity. Cem. Concr. Compos. 135 https://doi.org/10.1016/j.cemconcomp.2022.104834.

Gencel, O., Harja, M., Sarı, A., Hekimoğlu, G., Ustaoğlu, A., Sutcu, M., Erdogmus, E., Kaplan, G., Bayraktar, O.Y., 2022a. Development, characterization, and performance analysis of shape-stabilized phase change material included-geopolymer for passive thermal management of buildings. Int. J. Energy Res. 46, 21841–21855. https://doi.org/10.1002/er.8735.

Gencel, O., Ustaoglu, A., Benli, A., Hekimoğlu, G., Sarı, A., Erdogmus, E., Sutcu, M., Kaplan, G., Yavuz Bayraktar, O., 2022b. Investigation of physico-mechanical, thermal properties and solar thermoregulation performance of shape-stable attapulgite based composite phase change material in foam concrete. Sol. Energy 236, 51–62. https://doi.org/10.1016/j.solener.2022.02.042.

Haily, E., Ait Ousaleh, H., Zari, N., Faik, A., Bouhfid, R., Qaiss, A., 2023. Use of a form-stable phase change material to improve thermal properties of phosphate sludge-based geopolymer mortar. Construct. Build. Mater. 386 https://doi.org/10.1016/j.conbuildmat.2023.131570.

Han, Y., Yang, Y., Mallick, T., Wen, C., 2022. Nanoparticles to enhance melting performance of phase change materials for thermal energy storage. Nanomaterials 12, 1864. https://doi.org/10.3390/nano12111864.

Hao, L., Xiao, J., Sun, J., Xia, B., Cao, W., 2022. Thermal conductivity of 3D printed concrete with recycled fine aggregate composite phase change materials. J. Clean. Prod. 364 https://doi.org/10.1016/j.jclepro.2022.132598.

Hassan, A., Mourad, A.H.I., Rashid, Y., Ismail, N., Laghari, M.S., 2019a. Thermal and structural performance of geopolymer concrete containing phase change material encapsulated in expanded clay. Energy Build. 191, 72–81. https://doi.org/10.1016/j.enbuild.2019.03.005.

Hassan, A., Rashid, Y., Mourad, A.H.I., Ismail, N., Laghari, M.S., 2019b. Thermal and structural characterization of geopolymer-coated polyurethane foam-phase change material capsules/geopolymer concrete composites. Materials 12. https://doi.org/10.3390/MA12050796.

Iten, M., Liu, S., 2014. A work procedure of utilising PCMs as thermal storage systems based on air-TES systems. Energy Convers. Manag. https://doi.org/10.1016/j.enconman.2013.10.012.

Jiang, Z., Liu, G., 2015. Microencapsulation of ammonium polyphosphate with melamine-formaldehyde-tris(2-hydroxyethyl)isocyanurate resin and its flame retardancy in polypropylene. RSC Adv. 5, 88445–88455. https://doi.org/10.1039/c5ra14586d.

Jurčević, M., Nižetić, S., Čoko, D., Arıcı, M., Hoang, A.T., Giama, E., Papadopoulos, A., 2022. Techno-economic and environmental evaluation of photovoltaic-thermal collector design with pork fat as phase change material. Energy 254. https://doi.org/10.1016/j.energy.2022.124284.

Kasaeian, A., bahrami, L., Pourfayaz, F., Khodabandeh, E., Yan, W.M., 2017. Experimental studies on the applications of PCMs and nano-PCMs in buildings: a critical review. Energy Build. https://doi.org/10.1016/j.enbuild.2017.08.037.

Latibari, S.T., Mehrali, Mohammad, Mehrali, Mehdi, Mahlia, T.M.I., Metselaar, H.S.C., 2015. Fabrication and performances of microencapsulated palmitic acid with enhanced thermal properties. Energy Fuel. 29, 1010–1018. https://doi.org/10.1021/ef502840f.

Li, Z., Wang, L., Ma, G., 2020. Mechanical improvement of continuous steel microcable reinforced geopolymer composites for 3D printing subjected to different loading conditions. Compos. B Eng. 187 https://doi.org/10.1016/j.compositesb.2020.107796.

Liu, Z., Li, M., Kandasamy, R., Ho, J.Y., Wong, T.N., Li, H.K.H., Tan, M.J., 2022. Comprehensive investigations on printability and thermal performance of cementitious material incorporated with PCM under various conditions. Energy Convers. Manag. 261 https://doi.org/10.1016/j.enconman.2022.115667.

Lowke, D., Dini, E., Perrot, A., Weger, D., Gehlen, C., Dillenburger, B., 2018. Particle-bed 3D printing in concrete construction – possibilities and challenges. Cement Concr. Res. 112, 50–65. https://doi.org/10.1016/j.cemconres.2018.05.018.

Lucas, S.S., Ferreira, V.M., Aguiar, J.L.B. de, 2013. Latent heat storage in PCM containing mortars - study of microstructural modifications. Energy Build. 66, 724–731. https://doi.org/10.1016/j.enbuild.2013.07.060.

Ma, S., Yang, H., Zhao, S., He, P., Zhang, Z., Duan, X., Yang, Z., Jia, D., Zhou, Y., 2021. 3D-printing of architectured short carbon fiber-geopolymer composite. Compos. B Eng. 226 https://doi.org/10.1016/j.compositesb.2021.109348.

Mehrali, Mohammad, Latibari, S.T., Mehrali, Mehdi, Metselaar, H.S.C., Silakhori, M., 2013. Shape-stabilized phase change materials with high thermal conductivity based on paraffin/graphene oxide composite. Energy Convers. Manag. 67, 275–282. https://doi.org/10.1016/j.enconman.2012.11.023.

Merline, D.J., Vukusic, S., Abdala, A.A., 2013. Melamine formaldehyde: curing studies and reaction mechanism. Polym. J. 45, 413–419. https://doi.org/10.1038/pj.2012.162.

Milián, Y.E., Gutiérrez, A., Grágeda, M., Ushak, S., 2017. A review on encapsulation techniques for inorganic phase change materials and the influence on their thermophysical properties. Renew. Sustain. Energy Rev. https://doi.org/10.1016/j.rser.2017.01.159.

Mohseni, E., Tang, W., Khayat, K.H., Cui, H., 2020. Thermal performance and corrosion resistance of structural-functional concrete made with inorganic PCM. Construct. Build. Mater. 249 https://doi.org/10.1016/j.conbuildmat.2020.118768.

Palmer, B., Arshad, A., Yang, Y., Wen, C., 2023. Energy storage performance improvement of phase change materials-based triplex-tube heat exchanger (TTHX) using liquid–solid interface-informed fin configurations. Appl. Energy 333. https://doi.org/10.1016/j.apenergy.2022.120576.

Panda, B., Unluer, C., Tan, M.J., 2019. Extrusion and rheology characterization of geopolymer nanocomposites used in 3D printing. Compos. B Eng. 176 https://doi.org/10.1016/j.compositesb.2019.107290.

Parameshwaran, R., Naresh, R., Ram, V.V., Srinivas, P.v., 2021. Microencapsulated bio-based phase change material-micro concrete composite for thermal energy storage. J. Build. Eng. 39 https://doi.org/10.1016/j.jobe.2021.102247.

Paul, S.C., van Zijl, G.P.A.G., Gibson, I., 2018. A review of 3D concrete printing systems and materials properties: current status and future research prospects. Rapid Prototyp. J. https://doi.org/10.1108/RPJ-09-2016-0154.

Pilehvar, S., Cao, V.D., Szczotok, A.M., Valentini, L., Salvioni, D., Magistri, M., Pamies, R., Kjøniksen, A.L., 2017. Mechanical properties and microscale changes of geopolymer concrete and Portland cement concrete containing micro-encapsulated

phase change materials. Cement Concr. Res. 100, 341–349. https://doi.org/10.1016/j.cemconres.2017.07.012.
Pilehvar, S., Sanfelix, S.G., Szczotok, A.M., Rodríguez, J.F., Valentini, L., Lanzón, M., Pamies, R., Kjøniksen, A.L., 2020a. Effect of temperature on geopolymer and Portland cement composites modified with Micro-encapsulated Phase Change materials. Construct. Build. Mater. 252 https://doi.org/10.1016/j.conbuildmat.2020.119055.
Pilehvar, S., Sanfelix, S.G., Szczotok, A.M., Rodríguez, J.F., Valentini, L., Lanzón, M., Pamies, R., Kjøniksen, A.L., 2020b. Effect of temperature on geopolymer and Portland cement composites modified with Micro-encapsulated Phase Change materials. Construct. Build. Mater. 252 https://doi.org/10.1016/j.conbuildmat.2020.119055.
Pilehvar, S., Szczotok, A.M., Rodríguez, J.F., Valentini, L., Lanzón, M., Pamies, R., Kjøniksen, A.L., 2019a. Effect of freeze-thaw cycles on the mechanical behavior of geopolymer concrete and Portland cement concrete containing micro-encapsulated phase change materials. Construct. Build. Mater. 200, 94–103. https://doi.org/10.1016/j.conbuildmat.2018.12.057.
Pilehvar, S., Szczotok, A.M., Rodríguez, J.F., Valentini, L., Lanzón, M., Pamies, R., Kjøniksen, A.L., 2019b. Effect of freeze-thaw cycles on the mechanical behavior of geopolymer concrete and Portland cement concrete containing micro-encapsulated phase change materials. Construct. Build. Mater. 200, 94–103. https://doi.org/10.1016/j.conbuildmat.2018.12.057.
Ramakrishnan, S., Pasupathy, K., Sanjayan, J., 2021. Synthesis and properties of thermally enhanced aerated geopolymer concrete using form-stable phase change composite. J. Build. Eng. 40 https://doi.org/10.1016/j.jobe.2021.102756.
Ramakrishnan, S., Sanjayan, J., Wang, X., Alam, M., Wilson, J., 2015. A novel paraffin/expanded perlite composite phase change material for prevention of PCM leakage in cementitious composites. Appl. Energy 157, 85–94. https://doi.org/10.1016/j.apenergy.2015.08.019.
Ranjbar, N., Kuenzel, C., Gundlach, C., Kempen, P., Mehrali, M., 2023. Halloysite reinforced 3D-printable geopolymers. Cem. Concr. Compos. 136 https://doi.org/10.1016/j.cemconcomp.2022.104894.
Ranjbar, N., Mehrali, M., Kuenzel, C., Gundlach, C., Pedersen, D.B., Dolatshahi-Pirouz, A., Spangenberg, J., 2021. Rheological characterization of 3D printable geopolymers. Cement Concr. Res. 147 https://doi.org/10.1016/j.cemconres.2021.106498.
Ranjbar, N., Mehrali, Mehdi, Mehrali, Mohammad, Alengaram, U.J., Jumaat, M.Z., 2015. Graphene nanoplatelet-fly ash based geopolymer composites. Cement Concr. Res. 76, 222–231. https://doi.org/10.1016/j.cemconres.2015.06.003.
Rao, V.V., Parameshwaran, R., Ram, V.V., 2018. PCM-Mortar Based Construction Materials for Energy Efficient Buildings: A Review on Research Trends. Energy Build. https://doi.org/10.1016/j.enbuild.2017.09.098.
Ren, M., Liu, Y., Gao, X., 2020. Incorporation of phase change material and carbon nanofibers into lightweight aggregate concrete for thermal energy regulation in buildings. Energy 197. https://doi.org/10.1016/j.energy.2020.117262.
Rifaai, Y., Yahia, A., Mostafa, A., Aggoun, S., Kadri, E.H., 2019. Rheology of fly ash-based geopolymer: effect of NaOH concentration. Construct. Build. Mater. 223, 583–594. https://doi.org/10.1016/j.conbuildmat.2019.07.028.
Romagnoli, M., Sassatelli, P., Lassinantti Gualtieri, M., Tari, G., 2014. Rheological characterization of fly ash-based suspensions. Construct. Build. Mater. 65, 526–534. https://doi.org/10.1016/j.conbuildmat.2014.04.130.
Roussel, N., 2018. Rheological requirements for printable concretes. Cement Concr. Res. https://doi.org/10.1016/j.cemconres.2018.04.005.
Senthil, R., Punniakodi, B.M.S., Balasubramanian, D., Nguyen, X.P., Hoang, A.T., Nguyen, V.N., 2022. Numerical investigation on melting and energy storage density enhancement of phase change material in a horizontal cylindrical container. Int. J. Energy Res. 46, 19138–19158. https://doi.org/10.1002/er.8228.
Shadnia, R., Zhang, L., Li, P., 2015. Experimental study of geopolymer mortar with incorporated PCM. Construct. Build. Mater. 84, 95–102. https://doi.org/10.1016/j.conbuildmat.2015.03.066.
Shahzad, Q., Shen, J., Naseem, R., Yao, Y., Waqar, S., Liu, W., 2021. Influence of phase change material on concrete behavior for construction 3D printing. Construct. Build. Mater. 309 https://doi.org/10.1016/j.conbuildmat.2021.125121.
Shchukina, E.M., Graham, M., Zheng, Z., Shchukin, D.G., 2018. Nanoencapsulation of phase change materials for advanced thermal energy storage systems. Chem. Soc. Rev. https://doi.org/10.1039/c8cs00099a.
Singh, N.B., Kumar, M., Rai, S., 2019. Geopolymer cement and concrete: properties. In: Materials Today: Proceedings. Elsevier Ltd, pp. 743–748. https://doi.org/10.1016/j.matpr.2020.04.513.
Singh, P., Sharma, R.K., Ansu, A.K., Goyal, R., Sarı, A., Tyagi, V.v., 2021. A comprehensive review on development of eutectic organic phase change materials and their composites for low and medium range thermal energy storage applications. Sol. Energy Mater. Sol. Cell. https://doi.org/10.1016/j.solmat.2020.110955.
Tyagi, V.v., Pandey, A.K., Buddhi, D., Kothari, R., 2016. Thermal performance assessment of encapsulated PCM based thermal management system to reduce peak energy demand in buildings. Energy Build. 117, 44–52. https://doi.org/10.1016/j.enbuild.2016.01.042.
Tyagi, V.V., Buddhi, D., 2007. PCM thermal storage in buildings: a state of art. Renew. Sustain. Energy Rev. 11, 1146–1166. https://doi.org/10.1016/j.rser.2005.10.002.
Wahid, M.A., Hosseini, S.E., Hussen, H.M., Akeiber, H.J., Saud, S.N., Mohammad, A.T., 2017. An overview of phase change materials for construction architecture thermal management in hot and dry climate region. Appl. Therm. Eng. https://doi.org/10.1016/j.applthermaleng.2016.07.032.
Wang, D., Zhang, Xiaoxian, Luo, S., Li, S., 2012. Preparation and property analysis of melamine formaldehyde foam. Adv. Mater. Phys. Chem. 2, 63–67. https://doi.org/10.4236/ampc.2012.24b018.
Wei, Z., Falzone, G., Wang, B., Thiele, A., Puerta-Falla, G., Pilon, L., Neithalath, N., Sant, G., 2017. The durability of cementitious composites containing microencapsulated phase change materials. Cem. Concr. Compos. 81, 66–76. https://doi.org/10.1016/j.cemconcomp.2017.04.010.
Yan, P., Fan, W., Yang, Y., Ding, H., Arshad, A., Wen, C., 2022. Performance enhancement of phase change materials in triplex-tube latent heat energy storage system using novel fin configurations. Appl. Energy 327. https://doi.org/10.1016/j.apenergy.2022.120064.
Zhang, J., Cao, Z., Huang, S., Huang, X., Han, Y., Wen, C., Honoré Walther, J., Yang, Y., 2023. Solidification performance improvement of phase change materials for latent heat thermal energy storage using novel branch-structured fins and nanoparticles. Appl. Energy 342. https://doi.org/10.1016/j.apenergy.2023.121158.
Zhang, J., Cao, Z., Huang, S., Huang, X., Liang, K., Yang, Y., Zhang, H., Tian, M., Akrami, M., Wen, C., 2022. Improving the melting performance of phase change materials using novel fins and nanoparticles in tubular energy storage systems. Appl. Energy 322. https://doi.org/10.1016/j.apenergy.2022.119416.
Zhuang, X.Y., Chen, L., Komarneni, S., Zhou, C.H., Tong, D.S., Yang, H.M., Yu, W.H., Wang, H., 2016. Fly ash-based geopolymer: clean production, properties and applications. J. Clean. Prod. https://doi.org/10.1016/j.jclepro.2016.03.019.